Available online at www.sciencedirect.com
ScienceDirect
Journal of Power Sources 160 (2006) 1431–1435
JOURNAL OF POWER SOURCES
www.elsevier.com/locate/jpowsour

Electrochemical characteristics of iron carbide as an active material in alkaline batteries

Kiyoshi Ujimine, Atsushi Tsutsumi *

Department of Chemical System Engineering, The University of Tokyo, 7-3-1 Hongo, Bunkyo-ku, Tokyo 113-8656, Japan

Received 10 January 2006; received in revised form 4 March 2006; accepted 6 March 2006
Available online 15 May 2006

Abstract

Electrochemical properties of iron carbide (Fe_3C) for use as an alkaline battery anode were investigated during charge–discharge cycles. Results of electrochemical measurements and Mössbauer spectroscopy suggested that Fe_3C is oxidized irreversibly to Fe_3O_4 during discharge processes and that the produced Fe_3O_4 is subsequently changed to $Fe(OH)_2$ and Fe during the charging process, raising the discharge/charge capacity in further galvanostatic cycles. In addition, the electrode particles were observed to be less than 100 nm in diameter and to be highly dispersed on the surface of carbon black. These phenomena seems to be caused by dissolution and deposition of $Fe(OH)_2$ and Fe via intermediate iron species, leading to exposure of a fresh Fe_3C surface to the electrolyte after the second discharge.

Keywords: Alkaline battery anode; Iron carbide

1. Introduction

Electrical energy is a crucially important resource for modern civilization because it is easily transportable and is readily transformable to other kinds of energy: mechanical, chemical, light or heat. However, it is difficult to store electrical energy itself. This salient obstacle prevents more efficient use of electric energy, which could be achieved by stabilizing the power output of a power plant or by power generation using renewable energy sources. Efficient and large-scale electricity storage is necessary to solve these problems. From a cost-efficiency perspective, a simple and large battery system using an inexpensive active material would be suitable. Iron has been considered as a promising active material of alkaline secondary batteries because of its low cost, large specific capacity, and long-term durability [1–6]. For this study, we chose iron carbide Fe_3C, an inexpensive compound of iron, as an active material candidate. Usually, Fe_3C is synthesized through the reaction of iron oxide with natural gas using a fluidized bed reactor, which makes the energy consumed in Fe_3C production (15 GJ ton^{-1} [7]) less than that consumed in pure iron production (ca. 24 GJ ton^{-1} [8]). Therefore, the application of Fe_3C to an anode of an alkaline secondary battery instead of pure iron might save costs and energy required for producing a large-scale secondary battery, although the electrochemical characteristics of Fe_3C remain largely unknown. This study investigated the characteristics of Fe_3C as an active material of alkaline battery using electrochemical measurements, composition analysis and morphological observation.

2. Experimental

In this experiment, Fe_3C particles (Kawasaki Heavy Industries, Ltd.) of 0.1–0.5-mm diameter, which were produced by reduction of iron ore using methane in a fluidized bed reactor, were used as the active material. They contain 89.5 wt.% of Fe_3C and 10.5 wt.% of Fe_3O_4.

Particles of the active material were ground in a mortar and mixed with carbon black (Ketchen EC; Akzo Nobel Corp.) as a conductive material and polytetrafluoroethylene (PTFE) as a binder at the weight ratio of 20:4:1. After desiccation at 100 °C, the paste-like composite was applied on a 2-cm-diameter nickel foam disk, which was then pressed at 5 MPa for 5 min. Thickness of the prepared electrode was ca. 0.3 mm. A pure iron–carbon black electrode was fabricated similarly using electrolytic iron powder (Kanto Chemical Co. Inc.) of 0.1–0.2-mm

* Corresponding author. Tel.: +81 3 5841 7336; fax: +81 3 5841 7270.
E-mail address: tsutsumi@chemsys.t.u-tokyo.ac.jp (A. Tsutsumi).

0378-7753/$ – see front matter © 2006 Elsevier B.V. All rights reserved.
doi:10.1016/j.jpowsour.2006.03.002

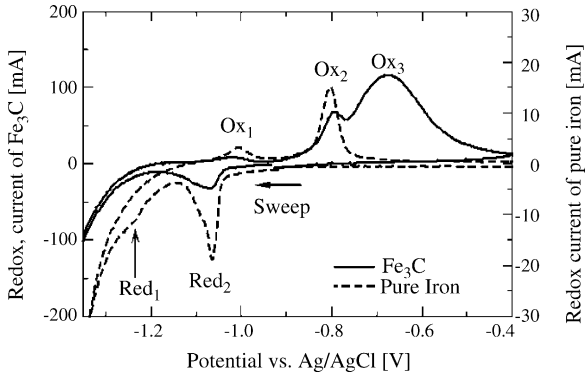

Fig. 1. Cyclic voltammogram of Fe_3C and pure iron. The potential sweep rate was 0.5 mA s^{-1}.

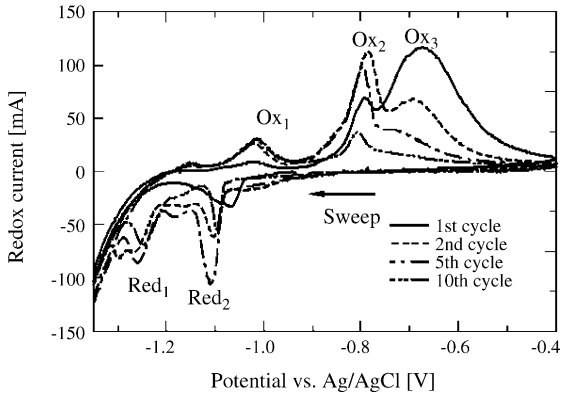

Fig. 2. Cyclic voltammograms of Fe_3C in discharge–charge cycles 1–10. The potential sweep rate was 0.5 mA s^{-1}.

diameter to compare electrochemical properties with those of Fe_3C.

A working electrode was soaked in the electrolyte of 6 mol dm^{-3} KOH solution for 2 h before electrochemical measurements. The electrolyte was connected electrically to a reference electrode, Ag/AgCl in saturated KCl aqueous solution, using a salt bridge of KCl. The electrolyte was kept at 25 °C during experimentation by circulating water around the electrochemical cell. Nickel wire was used as a counter electrode.

Galvanostatic potentiometry and cyclic voltammetry were carried out using a potentio/galvanostat (HZ-3000; Hokuto Denko Corp.). For galvanostatic potentiometry, the discharge and charge current density were 50 mA g^{-1}. In this measurement, the electrode was first oxidized until the potential reached −0.6 V versus Ag/AgCl in the discharge process, and then reduced until −1.2 V versus Ag/AgCl in the charge process. For cyclic voltammetry, the rest potential was −0.9 V versus Ag/AgCl and the potential scan rate was fixed at 0.5 mV s^{-1}.

To investigate the composition change of an active material in charge–discharge cycles, Mössbauer spectroscopy was performed. About 50 mg of the active material was mixed with 50 mg of boron nitride in a mortar. The mixture was pasted on a sample holder and measured using Mössbauer spectroscope (Laboratory Equipment Corp.). Composition of the sample was determined using calibration curve method. Calibration curves of Fe, Fe_3O_4 and Fe_3C were prepared using commercial products.

Morphology of Fe_3C particles was observed using scanning electron microscopy (SEM).

3. Results and discussion

Cyclic voltammograms of iron carbide and pure iron before the first discharge are shown in Fig. 1. In the case of pure iron, two pairs of reduction (Red)–oxidation (Ox) peaks are apparent, respectively, as Red_1/Ox_1 and Red_2/Ox_2 at −1.2 V/−1.0 V and −1.08 V/−0.8 V versus Ag/AgCl. These peaks are assigned, respectively, to the following reactions (1) and (2) of iron oxidation [4,5]:

$$Red_1/Ox_1: Fe(OH)_2 + 2e^- \rightleftarrows Fe + 2OH^- \quad (1)$$

$$Red_2/Ox_2: Fe_3O_4 + 4H_2O + 2e^- \rightleftarrows 3Fe(OH)_2 + 2OH^- . \quad (2)$$

In the case of iron carbide, a large and broad oxidation peak Ox_3 at −0.7 V versus Ag/AgCl was observed with a pair of small peaks that were similar to those of Ox_2/Red_2. Therefore, the Ox_3 peak is attributable to oxidation of Fe_3C. In addition, the appearance of peaks similar to Ox_2/Red_2 is inferred to result from the existence of Fe_3O_4 because Fe_3C particles contain 10.5 wt.% of Fe_3O_4.

Fig. 2 shows cyclic voltammograms of the first, second, fifth, and 10th cycles. Peaks are assignable, respectively, as Ox_1/Red_1, Ox_2/Red_2, and Ox_3. Changes of the current of each peak in the potential sweep cycles are shown in Fig. 3. The current of the oxidation peak Ox_3 resulting from the oxidation of Fe_3C decreased quickly along with the increase in the potential sweep cycle number and disappeared after the fifth cycle. This result indicates that Fe_3C oxidation is an irreversible reaction and that Fe_3C was consumed during the first five cycles. On the other hand, the current of Red_2 ($Fe_3O_4 \rightarrow Fe(OH)_2$) increased rapidly to a maximum at cycle 2 or 3 and then decreased gradually with increasing sweep cycle number, indicating an increase in the content of Fe_3O_4 in the reductive reaction shown in (2) after the first cycle. The current of both Red_2 and Ox_2 increased with increasing sweep

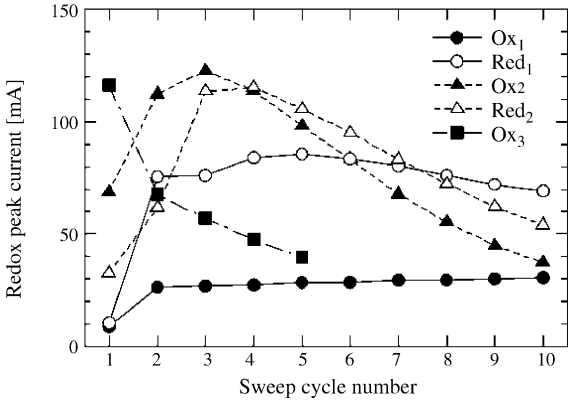

Fig. 3. Change of redox peak current in cyclic voltammetry.

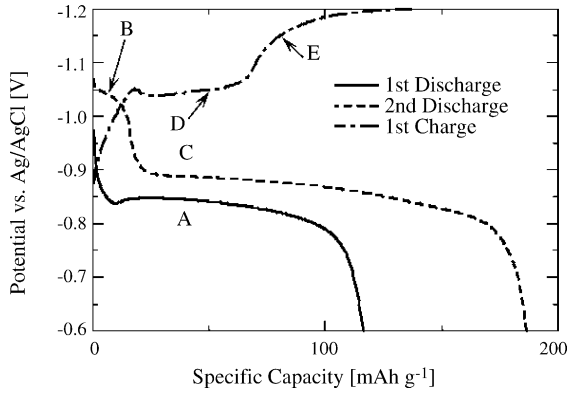

Fig. 4. Galvanostatic charge–discharge curves of Fe_3C. Charge and discharge current density were 50 mAg^{-1}.

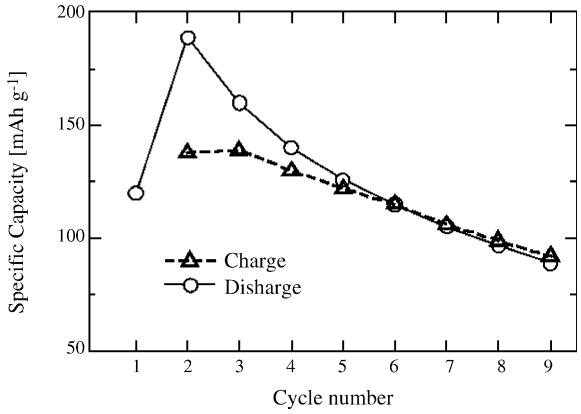

Fig. 5. Dependence of discharge/charge capacity of Fe_3C on the cycle number.

cycle number. Therefore, reaction (2) is inferred to take place reversibly. In addition, the current of Ox_1/Red_1 (redox reactions between $Fe(OH)_2$ and Fe) apparently increased at the second cycle and then leveled off. These results indicate that Fe_3C was oxidized irreversibly into Fe_3O_4 and that the Fe_3O_4 produced by oxidation of Fe_3C was reduced to Fe through $Fe(OH)_2$ in the cathodic sweep. It can therefore be concluded that the reversible redox reactions of $Fe_3O_4 \rightleftarrows Fe(OH)_2 \rightleftarrows Fe$ takes place after the oxidation of Fe_3C to produce Fe_3O_4.

Fig. 4 shows discharge and charge curves of Fe_3C in discharge–charge cycle measurements. In the curve of the first discharge, only one plateau, *A*, was observed at −0.85 V versus Ag/AgCl because of the oxidation of Fe_3C to produce Fe_3O_4. At the second discharge, two plateaus, *B* and *C*, appeared, respectively, at ca. −1.05 and −0.9 V versus Ag/AgCl. Plateaus *B* and *C* are considered to stem, respectively, from the electrochemical oxidation of Fe to $Fe(OH)_2$ (1) and $Fe(OH)_2$ to Fe_3O_4 (2). Because the rapid fall of potential occurs at the same value of plateau *A*, ca. −0.8 V versus Ag/AgCl, oxidation of Fe_3C is likely to take place in parallel with oxidation of $Fe(OH)_2$ to Fe_3O_4. In the charge curve, plateau *D* was observed between −1.05 and −1.1 V versus Ag/AgCl. The charging plateau *D* corresponds to the reduction of Fe_3O_4 produced through oxidation of Fe_3C. During charging, hydrogen bubbles were generated by water electrolysis in the region of −1.1 to −1.2 V versus Ag/AgCl (*E*). In that region, the reduction of $Fe(OH)_2$ to Fe also occurs in parallel with hydrogen evolution, indicating the low coulomb efficiency of $Fe(OH)_2$ reduction.

Table 1 shows the composition of Fe_3C particles before discharge–charge cycle measurement and after six discharge–charge cycles, as determined by Mössbauer spectroscopy. It is apparent that the Fe_3C content decreased and Fe_3O_4 content

Table 1
Composition of active material before and after charge–discharge cycle measurements

	Before (wt.%)	After (wt.%)
Fe_3C	89.5	73.0
Fe_3O_4	10.5	19.7
Fe	0.0	7.3

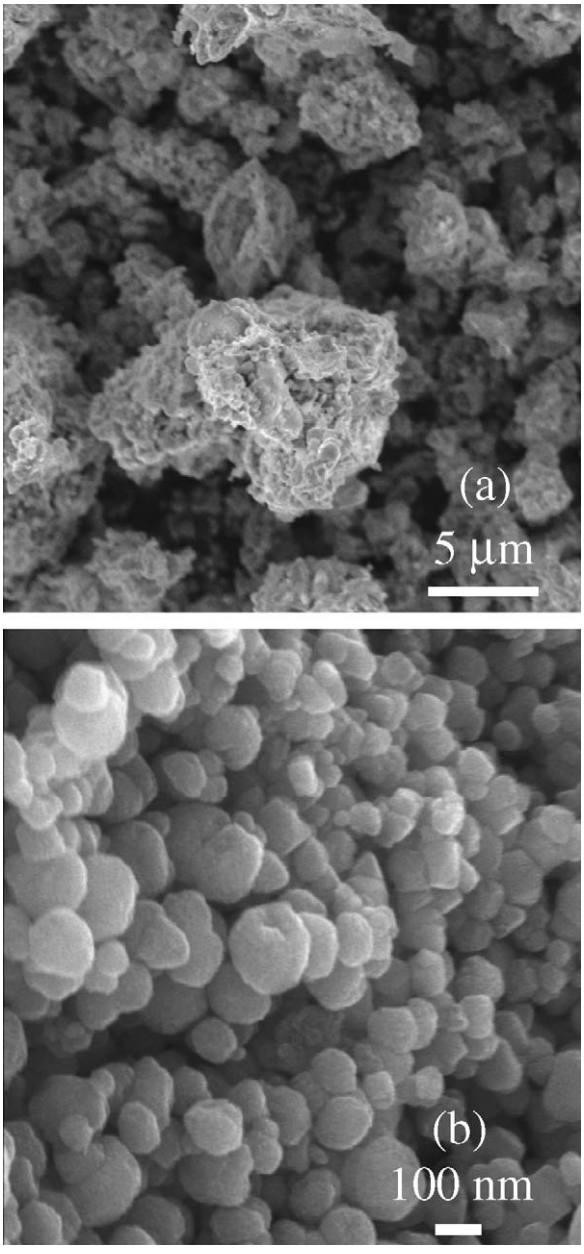

Fig. 6. SEM photographs of Fe_3C particles before (a) and after (b) charge–discharge measurements.

increased after discharge–charge cycles. In addition, the increase of Fe content in the sample was observed after cycle measurements. The increase of Fe_3O_4 content after discharge–charge cycles also suggests that Fe_3C is oxidized to Fe_3O_4 during discharge. In addition, the appearance of Fe is considered to result from the reduction of Fe_3O_4. From the results of Mössbauer spectroscopy, it is uncertain how carbon behaves in discharge–charge cycles. Considering the electrochemical stability of carbon, it is likely to remain unchanged in the electrode.

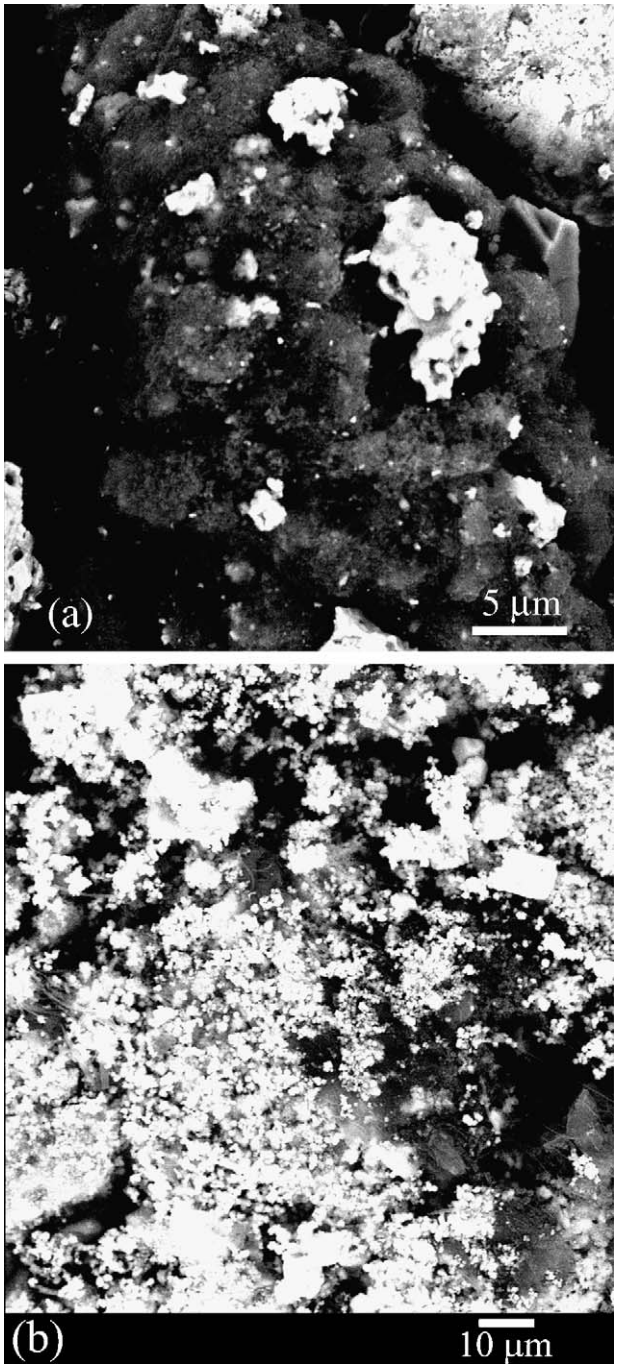

Fig. 7. Reflection electron images of an electrode before (a) and after (b) charge–discharge measurements. The bright spots in the images indicate the existence of iron species.

Fig. 5 shows the relationship between the cycle number and discharge capacity. The discharge capacity of the second discharge was observed to be about 1.5 times greater than that of the first discharge and even greater than the charge capacity of the first charge. In discharges 3–5, coulomb efficiency is apparently more than 100%, as in the second discharge. These results suggest that the structural change of electrode particles occurred and the fresh Fe_3C became exposed to electrolyte. After the second discharge, the capacity decreased quickly as the cycle number increased, implying the passivation of iron species.

Scanning electron microscopy (SEM) was performed to investigate the structural change of electrode particles. Some SEM images of samples before discharge–charge cycle measurement and after six discharge–charge cycles are shown in Fig. 6(a) and (b). Before discharge–charge cycle measurement, many pores with diameter of several 100 nm were observed on the surfaces of the 5–20 μm particles. In contrast, during charge–discharge cycles, the particles became more spherical than the original particles. Average diameters of electrode particles after six charge–discharge cycles were observed to be less than 100 nm. In addition, reflection electron images (Fig. 7(a) and (b)) indicate uniform dispersion of Fe_3C particles on the surface of carbon black particles after six charge–discharge cycles. Hang et al. [9,10] observed a similar phenomenon in the case of the mixture of Fe or Fe_2O_3 and carbon materials. They concluded that this phenomenon is attributable to the dissolution and deposition processes of Fe and $Fe(OH)_2$ via an intermediate species of iron: $HFeO_2^-$ [2,11]. Our measurements show that the Fe_3O_4 that is produced through oxidation of Fe_3C is reduced to Fe through $Fe(OH)_2$. Therefore, it is likely that the uniform dispersion of iron nanoparticles is attributable to the dissolution–deposition process between Fe and $Fe(OH)_2$ via $HFeO_2^-$. In addition, dissolution of these iron species seems to have caused the exposure of fresh Fe_3C surfaces, thereby creating more discharge capacity than the charge capacity.

In conclusion, all processes of charge–discharge in an Fe_3C electrode can be summarized as shown in Fig. 8. In the discharge process, Fe_3C is oxidized irreversibly to Fe_3O_4. During charging, the produced Fe_3O_4 is subsequently reduced to $Fe(OH)_2$ and Fe, contributing to the increased discharge

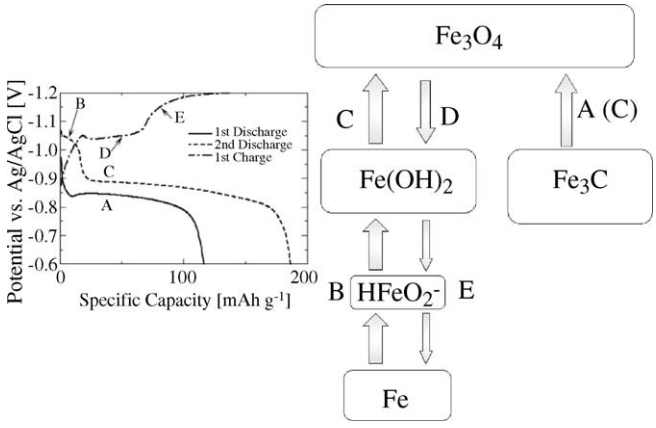

Fig. 8. Schematic diagram of the reaction of Fe_3C in alkaline electrolyte.

capacity after the second discharge. In the redox reaction of $Fe(OH)_2$ and Fe, they are likely to be dissolved and deposited through the intermediate ion of $HFeO_2^-$, thereby causing the uniform deposition of iron nanoparticles on the electrode surface.

4. Conclusions

Iron carbide (Fe_3C) was applied as the active material of an anode of an alkaline battery and the charge–discharge reaction scheme of Fe_3C was investigated. Results of cyclic voltammetry, galvanostatic discharge–charge measurement and Mössbauer spectroscopy indicated that Fe_3C was oxidized irreversibly into Fe_3O_4 during the discharge process and that the produced Fe_3O_4 was reduced to $Fe(OH)_2$ or Fe during the charge process. Results also showed that Fe and $Fe(OH)_2$ produced during the charge process were oxidized electrochemically after subsequent discharge in parallel with the electrochemical oxidation of Fe_3C. After discharge–charge cycles, Fe_3C particles were observed to change their shape to spherical particles with less than 100-nm diameter. It is likely that this result was caused by the dissolution–deposition process of $Fe(OH)_2$ and Fe via intermediate iron species. The authors infer that fresh surfaces of Fe_3C are exposed to alkaline electrolyte as a result of this dissolution–deposition process, exhibiting apparent coulomb efficiency of more than 100% in discharges 2–5.

Acknowledgements

The authors would like to thank Kawaju Techno Service Corp. for measuring samples using Mössbauer spectroscopy. The authors also thank Dr. Kazuo Tsutsumi of Kawasaki Heavy Industries, Ltd. for providing Fe_3C particles. The New Energy and Industrial Technology Development Organization (NEDO) funded this work.

References

[1] L. Ojefors, L. Carlsson, J. Power Sources 2 (1977/1978) 287–296.
[2] P. Periasamy, B.R. Babu, S. Venkatakrishna Iyer, J. Power Sources 58 (1996) 35–40.
[3] N. Jayalakshmi, V.S. Muralidharan, J. Power Sources 32 (1990) 341–351.
[4] M.K. Ravikumar, T.S. Balasubramanian, A.K. Shukla, J. Power Sources 56 (1995) 209–212.
[5] C.A. Caldas, M.C. Lopes, I.A. Carlos, J. Power Sources 74 (1998) 108–112.
[6] C.A.C. Souza, I.A. Carlos, M. Lopes, G.A. Finazzi, M. Rh de Almeida, J. Power Sources 132 (2004) 288–290.
[7] T. Ito, Master's thesis, University of Tokyo, 2003.
[8] R. Patela, W. Hutny, J.T. Price, Adv. Env. Res. 6 (2002) 157–170.
[9] B.T. Hang, M. Eashira, I. Watanabe, S. Okada, J.-I. Yamaki, S.-H. Yoon, I. Mochida, J. Power Sources 143 (2005) 256–264.
[10] B.T. Hang, T. Watanabe, M. Eashira, S. Okada, J.-I. Yamaki, S. Hata, S.-H. Yoon, I. Mochida, J. Power Sources 150 (2005) 261–271.
[11] R.D. Armstrong, I.T. Baurhoo, J. Electroanal. Chem. 34 (1972) 41–46.